

NANO EXPRESS

Open Access



The Photodetectors Based on Lateral Monolayer MoS₂/WS₂ Heterojunctions

Caihong Li¹ , Juntong Zhu², Wen Du¹, Yixuan Huang¹, Hao Xu^{3,4*}, Zhengang Zhai⁵ and Guifu Zou^{2*}

Abstract

Monolayer transition metal dichalcogenides (TMDs) show promising potential for next-generation optoelectronics due to excellent light capturing and photodetection capabilities. Photodetectors, as important components of sensing, imaging and communication systems, are able to perceive and convert optical signals to electrical signals. Herein, the large-area and high-quality lateral monolayer MoS₂/WS₂ heterojunctions were synthesized via the one-step liquid-phase chemical vapor deposition approach. Systematic characterization measurements have verified good uniformity and sharp interfaces of the channel materials. As a result, the photodetectors enhanced by the photogating effect can deliver competitive performance, including responsivity of ~567.6 A/W and detectivity of ~7.17 × 10¹¹ Jones. In addition, the 1/f noise obtained from the current power spectrum is not conducive to the development of photodetectors, which is considered as originating from charge carrier trapping/detrapping. Therefore, this work may contribute to efficient optoelectronic devices based on lateral monolayer TMD heterostructures.

Keywords: Lateral monolayer heterostructure, MoS₂/WS₂ heterojunction, Photodetector, Sharp interface

Introduction

Considering the almost half-a-trillion-dollar semiconductor-chip market, two-dimensional (2D) materials are currently one of the most feasible and promising candidates for extending Moore's law [1–5]. As a representative member of the 2D family, transition metal dichalcogenides (TMDs) have been intensively studied due to their distinctive optoelectronic properties and potential applications [6–12] in photodetection and light-emitting devices [13, 14]. Notably, the tunable bandgap, high carrier mobility, high optical absorption and atomically thin thickness, making TMDs appropriate channel materials for photodetectors, play a crucial role in optoelectronic or electronic devices [15, 16]. Although crystal defects in TMDs giving rise to the carrier trapping effect

can result in high photosensitivity, they can unavoidably lead to slow response speed yet [17]. In addition, some researchers propose the plasmonic enhancement to boost the limited light utilization of 2D materials [18–20]. Combining respective superiorities and showing unique electronic transport at the junction, TMDs heterostructures either lateral stitching or vertical stacking are presented [21]. Such heterostructures can tailor intrinsic electronic properties and improve the optical absorption [22], showing emerging and designable features [13, 23]. For example, the built-in electrical field [24] or energy level difference [25] induced by TMD heterostructures should accelerate photocarrier separation [26], suppress photocarrier recombination [17, 27] and lower dark current [28] as well, which is beneficial for achieving high-performance photodetection. Besides, Wang's group [29] has certified suppressed electron–hole (e–h) recombination in lateral heterostructures. As previously reported, the lateral heterostructures showed higher carrier mobility [30] whereas the vertical heterostructures usually increased the photoactive area [27] and/or enhanced current drive per area [31]. Moreover, the in-plane interfaces

*Correspondence: hao.xu.15@uestc.edu.cn; guifuzou@suda.edu.cn

² the College of Energy, Soochow Institute for Energy and Materials Innovations, and Key Laboratory of Advanced Carbon Materials and Wearable Energy Technologies of Jiangsu Province, Soochow University, Suzhou 215006, People's Republic of China

³ School of Physics, University of Electronic Science and Technology of China, Chengdu 610054, People's Republic of China

Full list of author information is available at the end of the article

of lateral heterostructures showed stronger emission intensity than both sides [14]. However, the suppressed photoluminescence (PL) emission could be observed in the vertical hetero-interface because of the reduced direct radiative recombination [32]. Additionally, both lateral and vertical TMDs heterostructures make it possible to create new excitonic transitions [14].

In terms of crystal lattice quality, MoX_2/WX_2 ($X = \text{S}, \text{Se}$ or Te) lateral heterojunctions could induce structural defects scarcely due to their similar honeycomb-like [33, 34] configuration and lattice parameters [34]. In addition, this kind of heterojunction can form type-II band alignment generally, which is desirable for high-efficiency photodetection [32, 34, 35]. According to the former work, lateral monolayer MoS_2/WS_2 heterojunction preferred to exhibit type-II band alignment with the valence band maximum (VBM) localized at WS_2 and the conduction band minimum (CBM) at MoS_2 [32, 34]. For instance, Wu's group have further reported that the VBM and CBM of MoS_2 are 0.39 eV and 0.35 eV lower than that of WS_2 , respectively [34]. Furthermore, the band offset between MoS_2 and WS_2 determining the band alignment could be estimated via their different d-orbital positions of Mo and W [34]. Vertical heterostructures can be prepared by mechanical transfer and stack, whereas lateral ones can be only achieved by growth methods [14]. Furthermore, vertical heterostructures, as previously reported, cannot be precise control and it is easily contaminated at the interfaces between layers [33]. Luckily, the lateral heterostructures can be synthesized by one-step method to reduce contaminations [28]. Nowadays the growth of large-area and high-quality lateral monolayer TMDs heterostructures has remained a great challenge [36]. Hence, high-quality and large-area lateral TMDs heterojunctions are significant and desired for the development of high-performance photodetectors.

Here, the lateral monolayer MoS_2/WS_2 heterojunctions with sharp interfaces and good uniformity via one-step liquid-phase CVD method are prepared and photodetectors are fabricated based on these heterostructures. The presented photodetectors can deliver high responsivity and detectivity of 567.6 A/W and 7.17×10^{11} Jones, respectively. This work demonstrates lateral monolayer MoS_2/WS_2 heterojunctions can serve as qualified candidates for next-generation optoelectronic applications.

Methods

Heterostructure Synthesis

0.05 g sodium tungstate, 0.5 g ammonium molybdate and 0.12 g NaOH (or KOH) particles were dissolved in 10 mL of deionized (DI) water to obtain precursor solution. The growth substrates (sapphire) were treated by piranha solution to improve the surface hydrophilicity,

and then the precursor solution was evenly spin-coated onto clean sapphire substrates. After that, the precursor covered sapphire and sulfur were placed on the heating center and upstream of a quartz tube, respectively. The heating center was ramped up to 700 °C in 40 min and maintained for 10 min to grow MoS_2 -OH bilayers (i.e. MoS_2 monolayer and a single layer of OH^- ions attached). Finally, the carrier gas was changed from Ar to Ar/ H_2 (5% H_2), and the heating center heated to 780 °C within 10 min and kept for 10 min to allow WS_2 to grow along the edges of MoS_2 -OH bilayers, forming MoS_2/WS_2 lateral heterostructures. The more details of the heterostructure synthesis refer to previous work [30].

Transfer Process

We used the polystyrene (PS)-assisted method to transfer WS_2/MoS_2 lateral heterostructures from sapphire to SiO_2/Si substrates. The PS solution (9 g of PS was dissolved in 100 mL of toluene) is first spin-coated on the heterostructures with 3500 rpm for 60 s, then the sample is baked at 90 °C for 10 min to eliminate toluene. After that, the WS_2/MoS_2 -PS film is obtained by a water droplet, and the floating WS_2/MoS_2 -PS film is then dredged up with a clean SiO_2/Si substrate. The WS_2/MoS_2 -PS- SiO_2/Si sample is baked at 80 °C for 1 h and then at 150 °C for 30 min to spread the polymer to eliminate possible wrinkles. Finally, the PS film is removed by rinsing with toluene several times to get WS_2/MoS_2 - SiO_2/Si samples.

Device Fabrication

The standard electron beam lithography (EBL) was used to define the markers and electrode patterns on the as-grown lateral monolayer MoS_2/WS_2 heterojunctions. The Ti/Au electrodes (10 nm/100 nm) were evaporated on the channel and lifted off in acetone. The device was thermal annealed at 400 °C for 2 h in vacuum and cooled down to room temperature rapidly.

Material Characterization

The optical images were captured with OLYMPUS microscope (LV100ND). The Raman, PL and AFM mapping images were measured with a Raman-AFM confocal spectrometer (Witec, alpha300 RA) with a laser of 532 nm.

Device Characterization

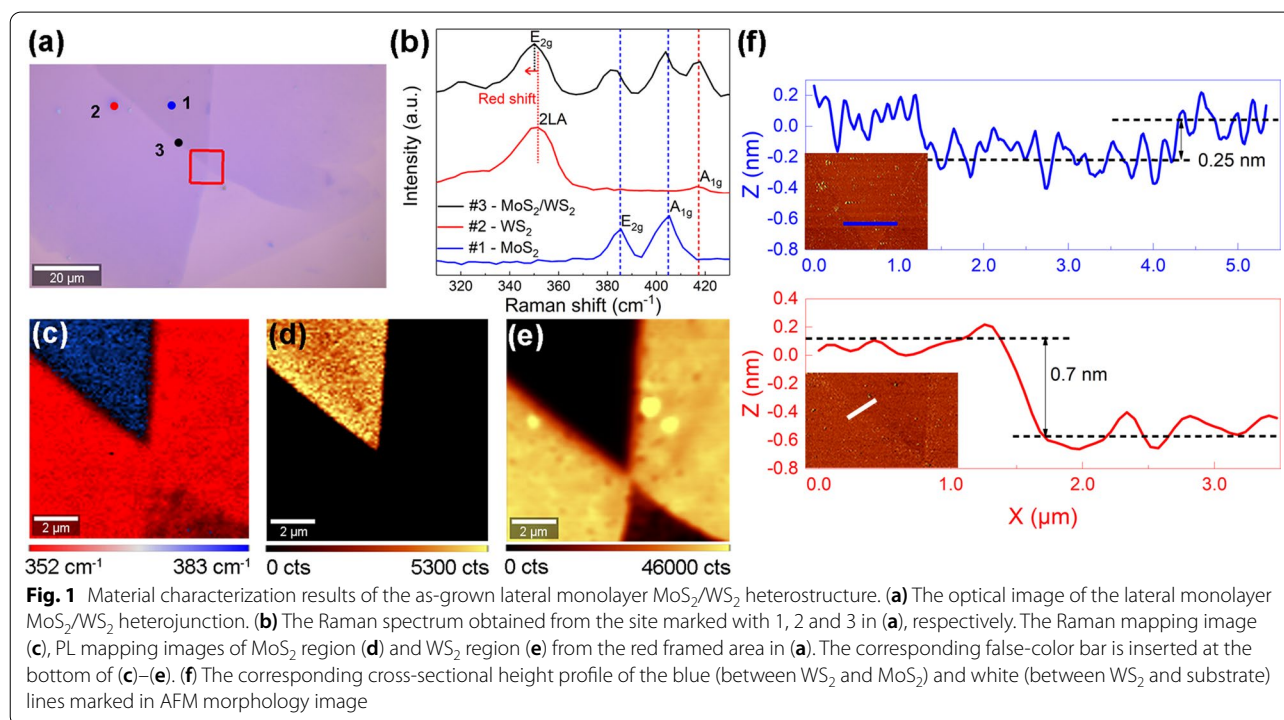
The optoelectronic properties of the photodetectors were measured with the SemiProbe probe station and a semiconductor parameter analyzer (Keithley 4200) and Platform Design Automation (PDA, FS-Pro). Different wavelength lasers as the light sources were used

to measure the photoresponse of the photodetectors. Different laser densities were determined with an irradiatometer.

Results and Discussion

Figure 1a shows the optical image of the CVD-grown lateral monolayer heterostructure, illustrated by the optical contrast. The corresponding Raman spectra obtained from the different positions marked 1 and 2 in Fig. 1a confirm the configuration of the inner MoS₂ (385.5 cm⁻¹ and 405.3 cm⁻¹) and outer WS₂ (351.5 cm⁻¹ and 416.5 cm⁻¹) in Fig. 1b [30]. High crystal quality of MoS₂ and WS₂ are implied because no oxidation peak observed in the corresponding Raman spectra [37]. Especially, the eigen-peaks of MoS₂ and WS₂ both were observed in the stitched interface marked 3 in Fig. 1a, indicating two materials form at the interface. In addition, the frequency difference between the E_{2g} mode and A_{1g} mode of MoS₂ is 19.8 cm⁻¹, suggesting monolayer one [30, 38, 39]. When considering WS₂, the peak intensity ratio of longitudinal acoustic mode (2LA) [40] at 352 cm⁻¹ to A_{1g} mode, i.e. I_{2LA}/I_{A1g}, is more accurate to verify the thickness than frequency difference [14]. The ratio was estimated to be ~2, in agreement with monolayer WS₂ measured by 532 nm laser [14]. The distinct red shift of E_{2g} mode (in-plane vibration) can be observed, resulted from alloying effect [41] in the lateral heterojunctions. Notably, this similar behavior were also observed in the

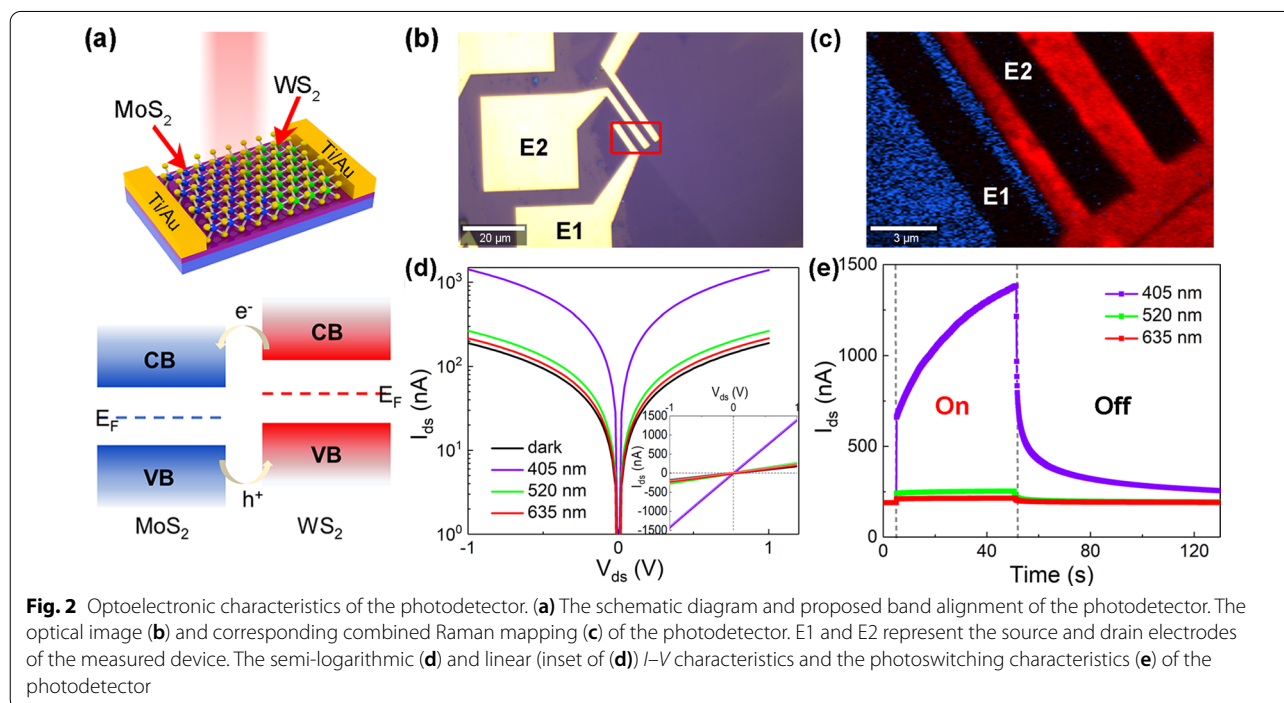
vertical heterojunctions, caused by dielectric screening and interlayer coupling [42]. Furthermore, the Raman mapping result in Fig. 1c with the blue region of MoS₂ and the red region of WS₂ indicates the seamless high-quality in-plane heterostructure [13, 43]. Figure 1d, e also demonstrate the configuration with MoS₂ inside and WS₂ outside by PL mapping, respectively [13]. Several points showing enhanced PL intensities in WS₂ region may be explained as carrier inhomogeneity caused by impurities or vacancies [14]. In addition, the stronger PL emissions at the interface than the MoS₂ region could be interpreted as the inhomogeneous distribution of carriers or higher photoinduced carrier recombination rate at the edges [14]. Both Raman and PL mapping suggest a sharp and well-stitched interface between MoS₂ and WS₂ [14, 44]. The thickness and surface morphology were measured by atomic force microscope (AFM) with trapping-mode. Note that few grain boundaries resulting in charge carrier scattering [45] are observed in material inside but edges indicating better electrical transport performance as shown in Fig. 1f [14, 46]. The thickness of WS₂ outside is ~0.7 nm (bottom) consistent with CVD-grown WS₂ monolayer reported previously [47], and the height difference between WS₂ and MoS₂ is about 0.25 nm (top), implying monolayered MoS₂ [47]. Overall, the above material characterization results can demonstrate the lateral monolayer MoS₂/WS₂ heterojunction with the sharp interface.



Photodetectors were fabricated using an EBL system based on the lateral MoS_2/WS_2 heterojunction. Figure 2a exhibits the schematic diagram (top) of the lateral heterojunction device and corresponding type-II band alignment (bottom). Accordingly, electrons and holes are transferred and confined in MoS_2 and WS_2 region through the interface, respectively, achieving the photoelectric conversion [13, 21, 24, 48]. We attribute this to the photogating effect, such as a special case of photoconductive effect [49]. The photogating effect can work as a local photogate modulating channel conductance [50]. The optical image of the device with the effective device area of $\sim 40 \mu\text{m}^2$ is described in Fig. 2b with E1 and E2 electrodes as the source and drain electrodes. In order to figure out the heterojunction configuration, combined Raman mapping was carried out (Fig. 2c), indicating the channel materials of lateral MoS_2/WS_2 heterojunction between the measured source and drain electrodes (E1 and E2) [28]. The blue, red and dark sections are MoS_2 , WS_2 and metal electrodes, respectively. Figure 2d shows the semi-logarithmic output characteristic curves of the lateral heterojunction under visible light with 405 nm, 520 nm and 635 nm, respectively. The inset in Fig. 2d reveals a linear I - V relationship between the channel and the electrodes [51–56]. The linear I - V character is conducive to achieving high responsivity but poor sensitivity of photodetectors due to a high dark current [57]. Additionally, the I_{ph} (i.e. $I_{\text{light}} - I_{\text{dark}}$) of the photodetector increases to 12.5 times of that before thermal annealing,

which maybe ascribe to decreased contact resistance [46, 58], removal of defects [59] and improved electrical conductivities [60]. Figure 2e depicts the photoswitching characteristics excited by the above wavelengths. The transient current rises rapidly when the light is on and drops as soon as the light is off, implying this photodetector can serve as a prompt light-activated switch [61].

The semi-logarithmic output characteristics with the same wavelength but varied laser power densities are depicted in Fig. 3a. As expected, photocurrent is enlarged as the laser power densities increase due to more induced photogenerated carriers [62]. Figure 3b shows the I - V curves with the same laser power density but different incident wavelengths (i.e. different light absorption amount and optical excitation energy). Although the shorter wavelength possesses fewer photons compared to the longer wavelength at the same laser power density. In this instance, the measured transient current increases with the decreases of the irradiation wavelength. This may be caused by the reduced optical absorption at the longer wavelength [63, 64]. Figure 3c describes the transient current under periodic laser illumination of 10 s, indicating a stable reproducible photoresponse [61]. For most low dimensional photodetector dominated by photogating effect, limited response speed and high responsivity can be obtained due to the prolonged excess carrier lifetime [50, 65]. The rise/fall time is defined as the time required for the photocurrent to rise/fall from 10%/90% of the stable value to 90%/10% [66, 67]. The relatively long



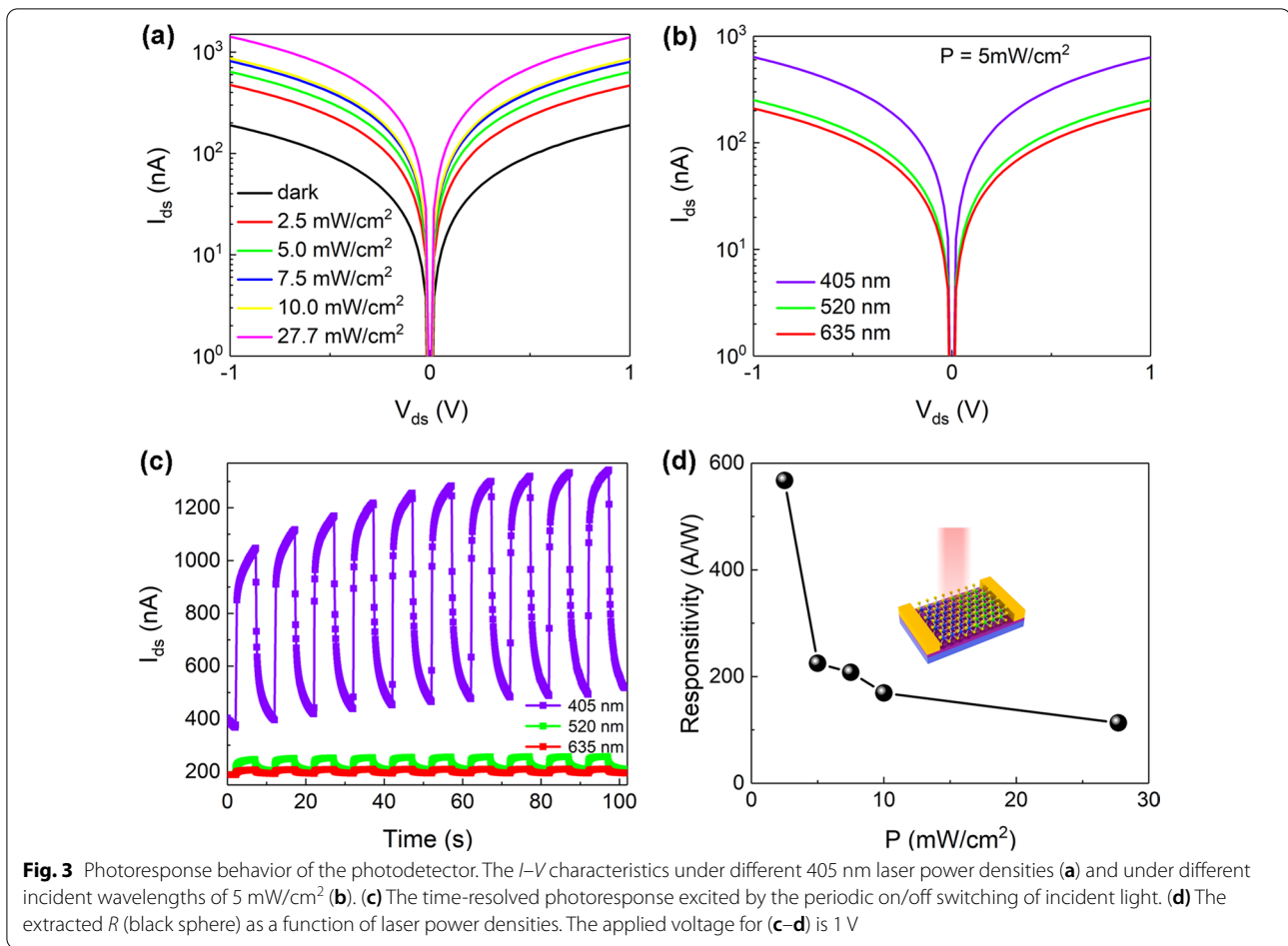


Fig. 3 Photoresponse behavior of the photodetector. The I - V characteristics under different 405 nm laser power densities (a) and under different incident wavelengths of 5 mW/cm² (b). (c) The time-resolved photoresponse excited by the periodic on/off switching of incident light. (d) The extracted R (black sphere) as a function of laser power densities. The applied voltage for (c-d) is 1 V

rise/fall time should be caused by slow carrier recombination, originated from laser illumination exciting many defective states [68]. Therefore, the response time including rise time and fall time was sacrificed by photogating effect because of the long-lived charge trapping processes [57]. Some researchers have proposed that the high-quality channel material which can offer a smooth and short path for carrier transfer and optimal device structure can improve the response speed [69, 70]. Indeed, the figures of merit of the photosensitive devices are mainly responsibility (R) and detectivity (D^*). R is calculated by the relations of

$$R = I_{ph}/(P \cdot S) \tag{1}$$

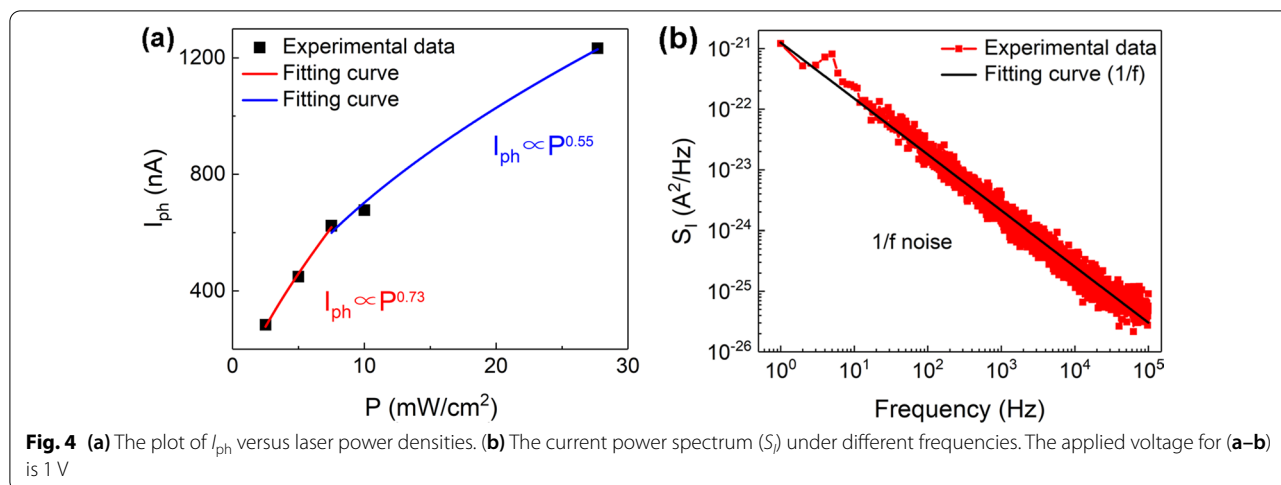
where P and S are laser power density and effective device area, respectively [62, 71, 72]. Figure 3d shows the corresponding values of R of the photodetector under different laser power densities. The champion R reaches up to ~567.6 A/W delivering the competitive

performance parameter. The high R is attributed to the suppressed photocarrier recombination in the heterostructure together with electron trapping in the MoS₂ region presumably [22]. The decreased R as the laser power density increased reveals the photogating effect in the photodetector further [73].

Moreover, photocurrent and laser power density follow the power-law equation:

$$I_{ph} = A P^\alpha \tag{2}$$

where A is a constant and $0 < \alpha < 1$. The value of α , obtained by fitting the curve of I_{ph} versus P in Fig. 4a, is related to the process of carrier capture, recombination and transfer [74, 75]. The sublinear relation between I_{ph} and P suggests the presence of the photogating effect in the device further [65]. The higher value of α (such as ~0.73) can be obtained when the lower power densities are applied due to reduced photocarrier recombination and the interactions between carriers [75, 76]. In contrast, higher power densities can result in a degraded α value of ~0.55 because of stronger



recombination losses and more trap states [77]. The precondition of the calculated D^* via the equation

$$D^* = R(S/2eI_{dark})^{1/2} \tag{3}$$

is that the photodetectors are limited by shot noise as the main noise source [49, 66, 78]. In order to further evaluate D^* more accurately, the noise current obtained in Fig. 4b is measured under different frequencies [74]. Figure 4b shows the typical 1/f noise [79] in our photodetectors, which is significant impediment to semiconductor industry from new materials. This kind of noise is

mainly resulted from the charged impurities and trapping sites in the conductive channel [57, 80]. A higher material quality and small structural defect density are desired for reducing the 1/f noise [81]. According to the formula of

$$D^* = R(S\Delta f)^{1/2} / I_{noise} \tag{4}$$

where Δf and I_{noise} are measurement bandwidth and noise current [79], the detectivity of the photodetector is about 7.17×10^{11} Jones. Table 1 has compared some selected representative photodetectors with corresponding photoresponse performance based on 2D materials.

Table 1 Some photoresponse performance of selected representative photodetectors based on 2D materials

Materials	Wavelength (nm)	Responsivity (A/W)	Detectivity (Jones)	References
monolayer WSe ₂	650	3.5×10^5	10^{14}	[82]
MoS ₂ -on-Au	1310	0.68	1.89×10^{12}	[83]
WSe ₂ /SnS ₂ heterostructure	550	244	1.29×10^{13}	[84]
MoS ₂ /MoSe ₂ heterojunction	610	1.3	2.6×10^{11}	[85]
WSe ₂ /WS ₂ heterojunction	532	300	7×10^2	[86]
SnSe ₂ /MoS ₂ heterostructure	500	9.1×10^3	9.3×10^{10}	[87]
WSe ₂ /BP/MoS ₂	532	6.32	1.25×10^{11}	[88]
CdS _x Se _(1-x)	450	703	3.41×10^{10}	[89]
SnS _{2x} Se _{2(1-x)}	633	6×10^3	8.2×10^{12}	[90]
WS ₂ /graphene nanosheets	480	1.15	2.06×10^9	[91]
SnS ₂ nanoflakes	400	354.4	2.0×10^{10}	[92]
SnSe ₂ flakes	530	1.1×10^3	1.01×10^{10}	[93]
Ca ₂ Nb ₃ O ₁₀	280	14.94	8.7×10^{13}	[72]
Sr ₂ Nb ₃ O ₁₀	270	1214	1.4×10^{14}	[71]
Graphene/WS ₂ heterostructure	400–700	10^6	3.8×10^{11}	[94]
P-MoS ₂ /N-MoS ₂	635	7×10^4	3.5×10^{14}	[95]
MoS ₂ /α-MoO _{3-x}	405	1.9×10^5	9.8×10^{16}	[96]
MoS ₂ /WS ₂ heterojunction	405	567.6	7.17×10^{11}	This work

The relatively high R and D^* of our photodetectors show great potential in optoelectronic devices.

Conclusions

In summary, a high-performance photodetector was developed based on the lateral monolayer MoS_2/WS_2 heterojunction. The size of the channel materials grown by the one-step liquid-phase CVD method reaches up to millimeter scale. Moreover, the high-quality channel materials with good uniformity and sharp interface were examined by systematic material characterizations and subsequent device measurements. Particularly, high responsivity of 567.6 A/W and detectivity of $\sim 10^{11}$ Jones are achieved for the photodetectors attributing to the photogating effect. The performance of the proposed lateral MoS_2/WS_2 heterojunction photodetectors is better than or comparable to the reported work [24, 62, 76, 78, 86, 97, 98]. In addition, we suppose the undesired $1/f$ noise arising from the trapping/detrapping of charge carriers maybe further reduced by high-quality and defect-less channel material. The facile one-step liquid-phase CVD growth and excellent optoelectronic performance of the photodetectors can motivate further research regarding optoelectronic devices based on lateral heterostructures.

Acknowledgements

We acknowledge engineer Wanghua Wu for helping PL data analysis.

Authors' contributions

CL and HX conceived and designed the reasearch project. JZ prepared the material. CL fabricated the device and performed the optical characteristics. CL and WD carried out the optoelectronic measurements. CL analyzed the data and wrote the manuscript with the contibution form YH and ZZ, HX and GZ supervised the project and modified manuscript. All authors read and approved the final manuscript.

Funding

This work was financially supported by the National Natural Science Foundation of China (G0562011530131), the National Key Research and Development Program of China (2019YFB2203400), the "111 Project" (B20030), the UESTC Shared Research Facilities of Electromagnetic Wave and Matter Interaction (Y0301901290100201), the Fundamental Research Funds for the Central Universities (ZYGX2019Z018), International Postdoctoral Exchange Fellowship Program (Talent-Introduction Program), China Postdoctoral Science Foundation (244125) and the Innovation Group Project of Sichuan Province (20CXTD0090).

Availability of data and materials

The datasets supporting the conclusions of this article are included in the article.

Delarations

Competing interests

The authors declasre they have no competing interests.

Author details

¹Institute of Fundamental and Frontier Sciences, University of Electronic Science and Technology of China, Chengdu 610054, People's Republic of China. ²the College of Energy, Soochow Institute for Energy and Materials Innovations, and Key Laboratory of Advanced Carbon Materials and Wearable Energy Technologies of Jiangsu Province, Soochow University, Suzhou 215006,

People's Republic of China. ³School of Physics, University of Electronic Science and Technology of China, Chengdu 610054, People's Republic of China. ⁴the State Key Laboratory of Electronic Thin Films and Integrated Devices, University of Electronic Science and Technology of China, Chengdu 610054, People's Republic of China. ⁵the 36th Research Institute of China Electronics Technology Group Corporation, Jiaxing 314033, People's Republic of China.

Received: 6 July 2021 Accepted: 21 July 2021

Published online: 31 July 2021

References

- Liu C, Chen H, Wang S, Liu Q, Jiang Y-G, Zhang DW, Liu M, Zhou P (2020) Two-dimensional materials for next-generation computing technologies. *Nat Nanotechnol* 15(7):545–557
- Wu G, Tian B, Liu L, Lv W, Wu S, Wang X, Chen Y, Li J, Wang Z, Wu S, Shen H, Lin T, Zhou P, Liu Q, Duan C, Zhang S, Meng X, Wu S, Hu W, Wang X, Chu J, Wang J (2020) Programmable transition metal dichalcogenide homo-junctions controlled by nonvolatile ferroelectric domains. *Nat Electron* 3(1):43–50
- Xu H, Ren A, Wu J, Wang Z (2020) Recent advances in 2D MXenes for photodetection. *Adv Funct Mater* 30(24):2000907
- Lan Y, Xia L-X, Huang T, Xu W, Huang G-F, Hu W, Huang W-Q (2020) Strain and electric field controllable Schottky barriers and contact types in grapheme– MoTe_2 van der Waals heterostructure. *Nanoscale Res Lett* 15(1):180
- Yu J, Zhong J, Kuang X, Zeng C, Cao L, Liu Y, Liu Z (2020) Dynamic control of high-range photoresponsivity in a graphene nanoribbon photodetector. *Nanoscale Res Lett* 15(1):124
- Xu H, Han X, Dai X, Liu W, Wu J, Zhu J, Kim D, Zou G, Sablon KA, Sergeev A, Guo Z, Liu H (2018) High detectivity and transparent few-layer MoS_2 /glassy-graphene heterostructure photodetectors. *Adv Mater* 30(13):1706561
- Xu H, Han X, Liu W, Liu P, Fang H, Li X, Li Z, Guo J, Xiang B, Hu W, Parkin IP, Wu J, Guo Z, Liu H (2020) Ambipolar and robust WSe_2 field-effect transistors utilizing self-assembled edge oxides. *Adv Mater Interfaces* 7(1):1901628
- Xu H, Zhu J, Zou G, Liu W, Li X, Li C, Ryu GH, Xu W, Han X, Guo Z, Warner JH, Wu J, Liu H (2020) Spatially bandgap-graded $\text{MoS}_{2(1-x)}\text{Se}_{2x}$ homojunctions for self-powered visible–near-infrared phototransistors. *Nano-Micro Lett* 12(1):26
- Du W, Yu P, Zhu J, Li C, Xu H, Zou J, Wu C, Wen Q, Ji H, Liu T, Li Y, Zou G, Wu J, Wang ZM (2020) An ultrathin MoSe_2 photodetector with near-perfect absorption. *Nanotechnology* 31(22):225201
- Du W, Li C, Sun J, Xu H, Yu P, Ren A, Wu J, Wang Z (2020) Nanolasers based on 2D materials. *Laser Photonics Rev* 14(12):2000271
- Xie Y, Wu E, Geng G, Zhang D, Hu X, Liu J (2021) Gate-tunable van der Waals heterostructure based on semimetallic WTe_2 and semiconducting MoTe_2 . *Appl Phys Lett* 118(13):133103
- Ning J, Zhou Y, Zhang J, Lu W, Dong J, Yan C, Wang D, Shen X, Feng X, Zhou H, Hao Y (2020) Self-driven photodetector based on a $\text{GaSe}/\text{MoSe}_2$ selenide van der Waals heterojunction with the hybrid contact. *Appl Phys Lett* 117(16):163104
- Cai Z, Liu B, Zou X, Cheng H-M (2018) Chemical vapor deposition growth and applications of two-dimensional materials and their heterostructures. *Chem Rev* 118(13):6091–6133
- Shen PC, Engineering MIOTDOE, Science C (2017) Large-area CVD growth of two-dimensional transition metal dichalcogenides and monolayer MoS_2 and WS_2 metal-oxide-semiconductor field-effect transistors. Massachusetts Institute of Technology, Department of Electrical Engineering and Computer Science, Cambridge
- Wang X, Lu Y, Zhang J, Zhang S, Chen T, Ou Q, Huang J (2021) Highly sensitive artificial visual array using transistors based on porphyrins and semiconductors. *Small* 17(2):2005491
- Zhou F, Zhou Z, Chen J, Choy TH, Wang J, Zhang N, Lin Z, Yu S, Kang J, Wong HSP, Chai Y (2019) Optoelectronic resistive random access memory for neuromorphic vision sensors. *Nat Nanotechnol* 14(8):776–782
- Wang P, Hu W (2019) Atomic layered 2d/3d heterostructure for sensitive photodetection. In: 2019 18th international conference on optical communications and networks (ICOON), pp 1–3

18. Li M-Y, Yu M, Jiang S, Liu S, Liu H, Xu H, Su D, Zhang G, Chen Y, Wu J (2020) Controllable 3D plasmonic nanostructures for high-quantum-efficiency UV photodetectors based on 2D and 0D materials. *Mater Horiz* 7(3):905–911
19. Liu S, Li M-Y, Zhang J, Su D, Huang Z, Kunwar S, Lee J (2020) Self-assembled Al nanostructure/ZnO quantum dot heterostructures for high responsivity and fast UV photodetector. *Nano-Micro Lett* 12(1):1–14
20. Liu S, Li M-Y, Su D, Yu M, Kan H, Liu H, Wang X, Jiang S (2018) Broad-band high-sensitivity ZnO colloidal quantum dots/self-assembled Au nanoantennas heterostructures photodetectors. *ACS Appl Mater Interfaces* 10(38):32516–32525
21. Liu Y, Zhang S, He J, Wang ZM, Liu Z (2019) Recent progress in the fabrication, properties, and devices of heterostructures based on 2D materials. *Nano-Micro Lett* 11(1):1–3
22. Nalwa HS (2020) A review of molybdenum disulfide (MoS_2) based photodetectors: from ultra-broadband, self-powered to flexible devices. *RSC Adv* 10(51):30529–30602
23. Neupane MR, Ruzmetov D, Burke R, Birdwell AG, Taylor D, Chin M, Regan TO, Crowne F, Nichols B, Shah P, Byrd E, Ivanov T (2018) Challenges and opportunities in integration of 2D materials on 3D substrates: materials and device perspectives. In: 2018 76th device research conference (DRC), pp 1–2
24. Wu W, Zhang Q, Zhou X, Li L, Su J, Wang F, Zhai T (2018) Self-powered photovoltaic photodetector established on lateral monolayer MoS_2 - WS_2 heterostructures. *Nano Energy* 51:45–53
25. Wang W, He J, Cao Y, Kong L, Zheng X, Wu Y, Chen X, Li S, Wu Z, Kang J (2017) Nonuniform effect of carrier separation efficiency and light absorption in type-II perovskite nanowire solar cells. *Nanoscale Res Lett*. <https://doi.org/10.1186/s11671-017-1912-4>
26. Song W, Chen J, Li Z, Fang X (2021) Self-powered MXene/GaN van der Waals heterojunction ultraviolet photodiodes with superhigh efficiency and stable current outputs. *Adv Mater* 33(27):2101059
27. Cheng H, Huang Y, Duan X (2016) Vertically stacked heterostructures for tunable photonic devices—from 2D materials to hybrid perovskites. In: 2016 Conference on lasers and electro-optics (CLEO), pp 1–2
28. Jia S, Jin Z, Zhang J, Yuan J, Chen W, Feng W, Hu P, Ajayan PM, Lou J (2020) Lateral monolayer MoSe_2 - WSe_2 p-n heterojunctions with giant built-in potentials. *Small* 16(34):2002263
29. Zhou Z, Zhang Y, Zhang X, Niu X, Wu G, Wang J (2020) Suppressing photoexcited electron-hole recombination in MoSe_2 - WSe_2 lateral heterostructures via interface-coupled state engineering: a time-domain ab initio study. *J Mater Chem A* 8(39):20621–20628
30. Zhu J, Li W, Huang R, Ma L, Sun H, Choi J-H, Zhang L, Cui Y, Zou G (2020) One-pot selective epitaxial growth of large WS_2 / MoS_2 lateral and vertical heterostructures. *J Am Chem Soc* 142(38):16276–16284
31. Akinwande D, Huyghebaert C, Wang C-H, Serna MI, Goossens S, Li L-J, Wong HSP, Koppens FHL (2019) Graphene and two-dimensional materials for silicon technology. *Nature* 573(7775):507–518
32. Yang W, Kawai H, Bosman M, Tang B, Chai J, Tay WL, Yang J, Seng HL, Zhu H, Gong H, Liu H, Goh KEJ, Wang S, Chi D (2018) Interlayer interactions in 2D WS_2 / MoS_2 heterostructures monolithically grown by in situ physical vapor deposition. *Nanoscale* 10(48):22927–22936
33. Zhang X, Huangfu L, Gu Z, Xiao S, Zhou J, Nan H, Gu X, Ostrikov K (2021) Controllable epitaxial growth of large-area MoS_2 / WS_2 vertical heterostructures by confined-space chemical vapor deposition. *Small* 17(18):2007312
34. Kang J, Tongay S, Zhou J, Li J, Wu J (2013) Band offsets and heterostructures of two-dimensional semiconductors. *Appl Phys Lett* 102(1):012111
35. Chen K, Wan X, Wen J, Xie W, Kang Z, Zeng X, Chen H, Xu J-B (2015) Electronic properties of MoS_2 - WS_2 heterostructures synthesized with two-step lateral epitaxial strategy. *ACS Nano* 9(10):9868–9876
36. Zavabeti A, Jannat A, Zhong L, Haidry AA, Yao Z, Ou JZ (2020) Two-dimensional materials in large-areas: synthesis. *Prop Appl Nano-Micro Lett* 12(1):66
37. Liu H, Xue Y (2021) Van Der Waals epitaxial growth and phase transition of layered FeSe nanocrystals. *Adv Mater* 33(17):2008456
38. Lee HS, Min S-W, Chang Y-G, Park MK, Nam T, Kim H, Kim JH, Ryu S, Im S (2012) MoS_2 nanosheet phototransistors with thickness-modulated optical energy gap. *Nano Lett* 12(7):3695–3700
39. Kim M, Seo J, Kim J, Moon JS, Lee J, Kim J-H, Kang J, Park H (2021) High-crystalline monolayer transition metal dichalcogenides films for wafer-scale electronics. *ACS Nano* 15(2):3038–3046
40. Berkdemir A, Gutiérrez HR, Botello-Méndez AR, Perea-López N, Elías AL, Chia C-I, Wang B, Crespi VH, López-Urías F, Charlier J-C, Terrones H, Terrones M (2013) Identification of individual and few layers of WS_2 using Raman spectroscopy. *Sci Rep* 3(1):1755
41. Sahoo PK, Memaran S, Xin Y, Balicas L, Gutiérrez HR (2018) One-pot growth of two-dimensional lateral heterostructures via sequential edge-epitaxy. *Nature* 553(7686):63–67
42. Liang L, Meunier V (2014) First-principles Raman spectra of MoS_2 , WS_2 and their heterostructures. *Nanoscale* 6(10):5394–5401
43. Zhang Z, Chen P, Duan X, Zang K, Luo J, Duan X (2017) Robust epitaxial growth of two-dimensional heterostructures, multiheterostructures, and superlattices. *Science* 357(6353):788–792
44. Ye K, Liu L, Liu Y, Nie A, Xiang K, Xiang J, Wang B, Wen F, Mu C, Zhao Z, Gong Y, Liu Z, Tian Y (2019) Lateral bilayer MoS_2 - WS_2 heterostructure photodetectors with high responsivity and detectivity. *Adv Opt Mater* 7(20):1900815
45. Tsen AW, Brown L, Levendoff MP, Ghahari F, Huang PY, Havener RW, Ruiz-Vargas CS, Muller DA, Kim P, Park J (2012) Tailoring electrical transport across grain boundaries in polycrystalline graphene. *Science* 336(6085):1143–1146
46. Wu M, Xiao Y, Zeng Y, Zhou Y, Zeng X, Zhang L, Liao W (2020) Synthesis of two-dimensional transition metal dichalcogenides for electronics and optoelectronics. *InfoMat* 3(4):362–396
47. Xiao J, Zhang Y, Chen H, Xu N, Deng S (2018) Enhanced performance of a monolayer MoS_2 / WSe_2 heterojunction as a photoelectrochemical cathode. *Nano-Micro Lett* 10(4):60
48. Cheng K, Guo Y, Han N, Su Y, Zhang J, Zhao J (2017) Lateral heterostructures of monolayer group-IV monochalcogenides: band alignment and electronic properties. *J Mater Chem C* 5(15):3788–3795
49. Shin GH, Park C, Lee KJ, Jin HJ, Choi S-Y (2020) Ultrasensitive phototransistor based on WSe_2 - MoS_2 van der Waals heterojunction. *Nano Lett* 20(8):5741–5748
50. Ramos M, Carrascoso F, Frisenda R, Gant P, Mañas-Valero S, Esteras DL, Baldoñi JJ, Coronado E, Castellanos-Gomez A, Calvo MR (2021) Ultra-broad spectral photo-response in FePS_3 air-stable devices. *NPJ 2D Mater Appl* 5(1):19
51. Shen P-C, Su C, Lin Y, Chou A-S, Cheng C-C, Park J-H, Chiu M-H, Lu A-Y, Tang H-L, Tavakoli MM, Pittner G, Ji X, Cai Z, Mao N, Wang J, Tung V, Li J, Bokor J, Zettl A, Wu C-I, Palacios T, Li L-J, Kong J (2021) Ultralow contact resistance between semimetal and monolayer semiconductors. *Nature* 593(7858):211–217
52. Wang Y, Kim JC, Wu RJ, Martinez J, Song X, Yang J, Zhao F, Mkhoyan A, Jeong HY, Chhowalla M (2019) Van der Waals contacts between three-dimensional metals and two-dimensional semiconductors. *Nature* 568(7750):70–74
53. Piprek G, Piprek J (2003) Semiconductor optoelectronic devices: introduction to physics and simulation. Elsevier Science, Philadelphia
54. Sze SM, Ng KK (2006) Physics of semiconductor devices, 3rd edn. Wiley, New Jersey
55. Fashandi H, Dahlqvist M, Lu J, Palisaitis J, Simak SI, Abrikosov IA, Rosen J, Hultman L, Andersson M, Lloyd Spetz A, Eklund P (2017) Synthesis of Ti_3AuC_2 , $\text{Ti}_3\text{Au}_2\text{C}_2$ and Ti_3IrC_2 by noble metal substitution reaction in Ti_3SiC_2 for high-temperature-stable Ohmic contacts to SiC. *Nat Mater* 16(8):814–818
56. Bittle EG, Basham JJ, Jackson TN, Jurchescu OD, Gundlach DJ (2016) Mobility overestimation due to gated contacts in organic field-effect transistors. *Nat Commun* 7(1):10908
57. Kufer D, Konstantatos G (2015) Highly sensitive, encapsulated MoS_2 photodetector with gate controllable gain and speed. *Nano Lett* 15(11):7307–7313
58. Zhu Y, Cao W, Fan Y, Deng Y, Xu C (2014) Effects of rapid thermal annealing on ohmic contact of AlGaIn/GaN HEMTs. *J Semicond* 35(2):026004
59. Park C-S (2018) Disorder induced transition of electrical properties of graphene by thermal annealing. *Results Phys* 9:1534–1536
60. Yang Q, Beers MH, Mehta V, Gao T, Parkinson D (2017) Effect of thermal annealing on the electrical conductivity of copper-tin polymer composites. *ACS Appl Mater Interfaces* 9(1):958–964

61. Pradhan B, Das S, Li J, Chowdhury F, Cherusseri J, Pandey D, Dev D, Krishnaprasad A, Barrios E, Towers A, Gesquiere A, Tetard L, Roy T, Thomas J (2020) Ultrasensitive and ultrathin phototransistors and photonic synapses using perovskite quantum dots grown from graphene lattice. *Sci Adv* 6(7):eaay5225
62. Yang T, Zheng B, Wang Z, Xu T, Pan C, Zou J, Zhang X, Qi Z, Liu H, Feng Y, Hu W, Miao F, Sun L, Duan X, Pan A (2017) Van der Waals epitaxial growth and optoelectronics of large-scale WSe_2/SnS_2 vertical bilayer p–n junctions. *Nat Commun* 8(1):1906
63. Bissett M, Worrall S, Kinloch I, Dryfe R (2016) Comparison of two-dimensional transition metal dichalcogenides for electrochemical supercapacitors. *Electrochim Acta* 201:30–37
64. Liu H-L, Shen C-C, Su S-H, Hsu C-L, Li M-Y, Li L-J (2014) Optical properties of monolayer transition metal dichalcogenides probed by spectroscopic ellipsometry. *Appl Phys Lett* 105(20):201905
65. Fang H, Hu W (2017) Photogating in low dimensional photodetectors. *Adv Sci* 4(12):1700323
66. Zhao Q, Wang W, Carrascoso-Plana F, Jie W, Wang T, Castellanos-Gomez A, Frisenda R (2020) The role of traps in the photocurrent generation mechanism in thin InSe photodetectors. *Mater Horiz* 7(1):252–262
67. Zhang T, Li S (2021) Self-powered all-inorganic perovskite photodetectors with fast response speed. *Nanoscale Res Lett* 16(1):6
68. Jiang J, Meng F, Cheng Q, Wang A, Chen Y, Qiao J, Pang J, Xu W, Ji H, Zhang Y, Zhang Q, Wang S, Feng X, Gu L, Liu H, Han L (2020) Low lattice mismatch InSe–Se vertical Van der Waals heterostructure for high-performance transistors via strong fermi-level depinning. *Small Methods* 4(8):2000238
69. Shi L, Chen K, Zhai A, Li G, Fan M, Hao Y, Zhu F, Zhang H, Cui Y (2021) Status and outlook of metal-inorganic semiconductor–metal photodetectors. *Laser Photonics Rev* 15(1):2000401
70. Li C, Li J, Li Z, Zhang H, Dang Y, Kong F (2021) High-performance photodetectors based on nanostructured perovskites. *Nanomaterials* 11(4):1038
71. Li S, Zhang Y, Yang W, Liu H, Fang X (2020) 2D Perovskite $Sr_2Nb_3O_{10}$ for high-performance UV photodetectors. *Adv Mater* 32(7):1905443
72. Zhang Y, Li S, Li Z, Liu H, Liu X, Chen J, Fang X (2021) High-performance two-dimensional perovskite $Ca_2Nb_3O_{10}$ UV photodetectors. *Nano Lett* 21(1):382–388
73. Lan H-Y, Hsieh Y-H, Chiao Z-Y, Jariwala D, Shih M-H, Yen T-J, Hess O, Lu Y-J (2021) Gate-tunable plasmon-enhanced photodetection in a monolayer MoS_2 phototransistor with ultrahigh photoresponsivity. *Nano Lett* 21:3083
74. Zhao Z, Wu D, Guo J, Wu E, Jia C, Shi Z, Tian Y, Li X, Tian Y (2019) Synthesis of large-area 2D WS_2 films and fabrication of a heterostructure for self-powered ultraviolet photodetection and imaging applications. *J Mater Chem C* 7(39):12121–12126
75. Cao R, Xu J, Shi S, Chen J, Liu D, Bu Y, Zhang X, Yin S, Li L (2020) High-performance self-powered ultraviolet photodetectors based on mixed-dimensional heterostructure arrays formed from NiO nanosheets and TiO_2 nanorods. *J Mater Chem C* 8(28):9646–9654
76. Zeng L, Tao L, Tang C, Zhou B, Long H, Chai Y, Lau SP, Tsang YH (2016) High-responsivity UV–Vis photodetector based on transferable WS_2 film deposited by magnetron sputtering. *Sci Rep* 6:20343
77. Natali D, Caironi M (2016) 7—Organic photodetectors. In: Nabet B (ed) *Photodetectors*. Woodhead Publishing, Sawston, pp 195–254
78. Ren A, Zou J, Lai H, Huang Y, Yuan L, Xu H, Shen K, Wang H, Wei S, Wang Y, Hao X, Zhang J, Zhao D, Wu J, Wang Z (2020) Direct laser-patterned MXene–perovskite image sensor arrays for visible–near infrared photodetection. *Mater Horiz* 7(7):1901–1911
79. Schneider HLHC (2007) *Quantum well infrared photodetectors: physics and applications*. Springer, Berlin
80. Macucci M, Marconcini P (2020) Theoretical comparison between the flicker noise behavior of graphene and of ordinary semiconductors. *J Sens* 2020:2850268
81. Balandin AA (2013) Low-frequency $1/f$ noise in graphene devices. *Nat Nanotechnol* 8(8):549–555
82. Zhang W, Chiu M-H, Chen C-H, Chen W, Li L-J, Wee ATS (2014) Role of metal contacts in high-performance phototransistors based on WSe_2 monolayers. *ACS Nano* 8(8):8653–8661
83. Mao Y, Xu P, Wu Q, Xiong J, Peng R, Huang W, Chen S, Wu Z, Li C (2021) Self-powered high-detectivity lateral MoS_2 schottky photodetectors for near-infrared operation. *Adv Electron Mater* 7(3):2001138
84. Zhou X, Hu X, Zhou S, Song H, Zhang Q, Pi L, Li L, Li H, Lü J, Zhai T (2018) Tunneling diode based on WSe_2/SnS_2 heterostructure incorporating high detectivity and responsivity. *Adv Mater* 30(7):1703286
85. Chen X, Qiu Y, Yang H, Liu G, Zheng W, Feng W, Cao W, Hu W, Hu P (2017) In-plane mosaic potential growth of large-area 2D layered semiconductors MoS_2 – $MoSe_2$ lateral heterostructures and photodetector application. *ACS Appl Mater Interfaces* 9(2):1684–1691
86. Tsai T-H, Liang Z-Y, Lin Y-C, Wang C-C, Lin K-I, Suenaga K, Chiu P-W (2020) Photogating WS_2 photodetectors using embedded WSe_2 charge puddles. *ACS Nano* 14(4):4559–4566
87. Zhou X, Zhou N, Li C, Song H, Zhang Q, Hu X, Gan L, Li H, Lü J, Luo J, Xiong J, Zhai T (2017) Vertical heterostructures based on $SnSe_2/MoS_2$ for high performance photodetectors. *2D Mater* 4(2):025048
88. Li H, Ye L, Xu J (2017) High-performance broadband floating-base bipolar phototransistor based on $WSe_2/BP/MoS_2$ heterostructure. *ACS Photonics* 4(4):823–829
89. Xia J, Zhao Y-X, Wang L, Li X-Z, Gu Y-Y, Cheng H-Q, Meng X-M (2017) van der Waals epitaxial two-dimensional CdS_xSe_{1-x} semiconductor alloys with tunable-composition and application to flexible optoelectronics. *Nanoscale* 9(36):13786–13793
90. Perumal P, Ulaganathan RK, Sankar R, Liao Y-M, Sun T-M, Chu M-W, Chou FC, Chen Y-T, Shih M-H, Chen Y-F (2016) Ultra-thin layered ternary single crystals $[Sn(S_xSe_{1-x})_2]$ with bandgap engineering for high performance phototransistors on versatile substrates. *Adv Funct Mater* 26(21):3630–3638
91. Alzakia FI, Tang B, Pennycook SJ, Tan SC (2020) Engineering the photoreponse of liquid-exfoliated 2D materials by size selection and controlled mixing for an ultrasensitive and ultrasensitive photodetector. *Mater Horiz* 7(12):3325–3338
92. Jia X, Tang C, Pan R, Long Y, Gu C, Li J (2018) Thickness-dependently enhanced photodetection performance of vertically grown SnS_2 nanoflakes with large size and high production. *ACS Appl Mater Interfaces* 10(21):18073–18081
93. Zhou X, Gan L, Tian W, Zhang Q, Jin S, Li H, Bando Y, Golberg D, Zhai T (2015) Ultrathin $SnSe_2$ flakes grown by chemical vapor deposition for high-performance photodetectors. *Adv Mater* 27(48):8035–8041
94. Mehew JD, Unal S, Torres Alonso E, Jones GF, Fadhil Ramadhan S, Craciun MF, Russo S (2017) Fast and highly sensitive ionic-polymer-gated WS_2 –graphene photodetectors. *Adv Mater* 29(23):1700222
95. Huo N, Konstantatos G (2017) Ultrasensitive all-2D MoS_2 phototransistors enabled by an out-of-plane MoS_2 PN homojunction. *Nat Commun* 8(1):572
96. Feng S, Liu C, Zhu Q, Su X, Qian W, Sun Y, Wang C, Li B, Chen M, Chen L, Chen W, Zhang L, Zhen C, Wang F, Ren W, Yin L, Wang X, Cheng H-M, Sun D-M (2021) An ultrasensitive molybdenum-based double-heterojunction phototransistor. *Nat Commun* 12(1):4094
97. Zhang D-D, Yu R-M (2019) Perovskite- WS_2 nanosheet composite optical absorbers on graphene as high-performance phototransistors. *Front Chem*. <https://doi.org/10.3389/fchem.2019.00257>
98. Lan C, Zhou Z, Zhou Z, Li C, Shu L, Shen L, Li D, Dong R, Yip S, Ho JC (2018) Wafer-scale synthesis of monolayer WS_2 for high-performance flexible photodetectors by enhanced chemical vapor deposition. *Nano Res* 11(6):3371–3384

Publisher's Note

Springer Nature remains neutral with regard to jurisdictional claims in published maps and institutional affiliations.